J|A|C|S ARTICLES

Published on Web 08/30/2010

Transition State Analysis of Thymidine Hydrolysis by Human Thymidine Phosphorylase

Phillip A. Schwartz, Mathew J. Vetticatt, and Vern L. Schramm*

Department of Biochemistry, Albert Einstein College of Medicine, 1300 Morris Park Avenue, Bronx, New York 10461

Received June 9, 2010; E-mail: vern.schramm@einstein.yu.edu

Abstract: Human thymidine phosphorylase (hTP) is responsible for thymidine (dT) homeostasis, and its action promotes angiogenesis. In the absence of phosphate, hTP catalyzes a slow hydrolytic depyrimidination of dT yielding thymine and 2-deoxyribose (dRib). Its transition state was characterized using multiple kinetic isotope effect (KIE) measurements. Isotopically enriched thymidines were synthesized enzymatically from glucose or (deoxy)ribose, and intrinsic KIEs were used to interpret the transition state structure. KIEs from [1′-^{14}C]-, [1-^{15}N]-, [1′-^{3}H]-, [2′*R*-^{3}H]-, [2′*S*-^{3}H]-, [4′-^{3}H]-, and [5′-^{3}H]dTs provided values of 1.033 ± 0.002, 1.004 ± 0.002, 1.325 ± 0.003, 1.101 ± 0.004, 1.087 ± 0.005, 1.040 ± 0.003, and 1.033 ± 0.003, respectively. Transition state analysis revealed a stepwise mechanism with a 2-deoxyribocation formed early and a higher energetic barrier for nucleophilic attack of a water molecule on the high energy intermediate. An equilibrium exists between the deoxyribocation and reactants prior to the irreversible nucleophilic attack by water. The results establish activation of the thymine leaving group without requirement for phosphate. A transition state constrained to match the intrinsic KIEs was found using density functional theory. An active site histidine (His116) is implicated as the catalytic base for activation of the water nucleophile at the rate-limiting transition state. The distance between the water nucleophile and the anomeric carbon (r_{C-O}) is predicted to be 2.3 Å at the transition state. The transition state model predicts that deoxyribose adopts a mild 3′-*endo* conformation during nucleophilic capture. These results differ from the concerted bimolecular mechanism reported for the arsenolytic reaction (Birck, M. R.; Schramm, V. L. *J. Am. Chem. Soc.* **2004**, *126*, 2447−2453).

Human thymidine phosphorylase (hTP)[1] catalyzes the reversible phosphorolytic depyrimidination of thymidine (dT) forming 2-deoxy-α-D-ribose 1-phosphate and thymine[2] and participates in dT homeostasis in cells. hTP is also known as platelet-derived endothelial cell growth factor (PD-ECGF) or gliostatin and also promotes angiogenesis through 2-deoxyribose formation.[3,4] The angiogenic activity of hTP plays a significant role in tumor biology, promoting new capillary blood vessel formation in certain cancers.[5,6] High levels of hTP expression in tumor cells have been correlated with poor prognoses. Inhibition of the enzyme has been investigated as a chemotherapeutic strategy to decrease angiogenesis, slow tumor growth, and reduce metastases.[7] Additionally, hTP plays a role in the catabolic inactivation of antiproliferative agents such as 5-trifluorothymidine (TFT) and 2′-deoxy-5-fluorouridine (5FdU).[8,9] Administration of an hTP inhibitor in combination with these drugs is proposed to increase their efficacy, thereby allowing reduced dosage and decreased off-target toxicity.[10]

Studies of glycosydic bond cleavage reactions have provided an emerging mechanistic understanding of the diverse reactions catalyzed by *O*-glycosidases (e.g., polysaccharide synthesis and hydrolysis) and *N*-glycosidases (e.g., the depurination and depyrimidination reactions of furanosides).[11−14] A unifying theme among these nucleophilic displacement reactions is formation of oxocarbenium ion intermediates or oxocarbenium ion-*like* transition states.[11] Reactions involving deoxynucleosides are under-represented in the study of glycosidic bond cleavage. Here we apply multiple intrinsic kinetic isotope effects (KIEs) and quantum chemistry to understand the transition state of hTP.[11,15] Intrinsic KIEs are influenced by motion along the reaction coordinate and the geometry of adjacent atoms at the

(1) Abbreviations: dAMP, deoxyadenosine monophosphate; dRib, 2-deoxyribose; dT, thymidine; EIE, equilibrium isotope effect; 5FdU, 2′-deoxy-5-fluorouridine; hTP, human thymidine phosphorylase; KIEs, kinetic isotope effects; PD-ECGF, platelet-derived endothelial cell growth factor; TFT, 5-trifluorothymidine; TPI, thymidine phosphorylase inhibitor (5-chloro-6-[1-(2-iminopyrrolidinyl)methyl]uracil hydrochloride); UDG, uracil DNA gycosylase.

(2) Friedkin, M.; Roberts, D. *J. Biol. Chem.* **1954**, *207*, 245–256.
(3) Brown, N. S.; Bicknell, R. *Biochem. J.* **1998**, *334* (1), 1–8.
(4) Ishikawa, F.; Miyazono, K.; Hellman, U.; Drexler, H.; Wernstedt, C.; Hagiwara, K.; Usuki, K.; Takaku, F.; Risau, W.; Heldin, C. H. *Nature* **1989**, *338*, 557–562.
(5) de Bruin, M.; Temmink, O. H.; Hoekman, K.; Pinedo, H. M.; Peters, G. J. *Cancer Therapy* **2006**, *4*, 99–124.
(6) Bijnsdorp, I. V.; de Bruin, M.; Laan, A. C.; Fukushima, M.; Peters, G. J. *Nucleosides, Nucleotides Nucleic Acids* **2008**, *27*, 681–691.
(7) Focher, F.; Spadari, S. *Curr. Cancer Drug Targets* **2001**, *1*, 141–153.
(8) Cole, C.; Foster, A. J.; Freeman, S.; Jaffar, M.; Murray, P. E.; Strafford, I. J. *Anti-Cancer Drug Des.* **1999**, *14*, 383–392.
(9) Fukushima, M.; Suzuki, N.; Emura, T.; Yano, S.; Kazuno, H.; Tada, Y.; Yamada, Y.; Asao, T. *Biochem. Pharmacol.* **2000**, *59*, 1227–1236.
(10) Temmink, O. H.; Emura, T.; de Bruin, M.; Fukushima, M.; Peters, G. J. *Cancer Sci.* **2007**, *98*, 779–789.
(11) Berti, P. J.; Tanaka, K. S. *Adv. Phys. Org. Chem.* **2002**, *37*, 239–314.
(12) Capon, B. *Chem. Rev.* **1969**, *69*, 407–498.
(13) Zechel, D. L.; Withers, S. G. *Acc. Chem. Res.* **2000**, *33*, 11–18.
(14) Berti, P. J.; McCann, J. A. *Chem. Rev.* **2006**, *106*, 506–555.
(15) Schramm, V. L. *Acc. Chem. Res.* **2003**, *36*, 588–596.

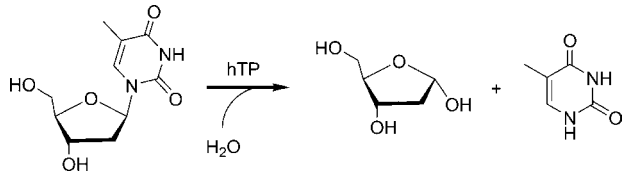

Figure 1. hTP-catalyzed hydrolytic depyrimidination of dT.

transition state. For nucleophilic substitution reactions, this allows a concerted bimolecular process (A_ND_N) to be distinguished from a stepwise process ($D_N{*}A_N$).[16] Furthermore, stepwise mechanisms can be resolved with respect to being rate-limiting at leaving group departure (the first step, $D_N^{\ddagger}{*}A_N$) or at nucleophilic attack (the second step, $D_N{*}A_N^{\ddagger}$).

The physiological reaction of hTP uses inorganic phosphate as the nucleophile, but this reaction is not amenable to KIE approaches because of kinetic complexity obscuring the chemical step(s). The slow hydrolytic reaction permits intrinsic KIE measurements (Figure 1). Multiple KIEs are used to demonstrate this reaction to proceed through a stepwise $D_N{*}A_N^{\ddagger}$ mechanism. The V/K KIEs determined for this reaction are the product of the KIEs on the nucleophilic attack (A_N) step and the equilibrium isotope effect (EIE) from the equilibrium between the 2-deoxyribosyl oxocarbenium ion intermediate and free dT. This transition state differs from that reported earlier for the reaction using AsO_4 as the substrate analogue.[17]

Materials and Methods

Materials. ^{3}H- and ^{14}C-labeled riboses and glucoses and [5′-^{3}H]dT were purchased from American Radiolabeled Chemicals. ^{15}N-labeled thymine and thymidine phosphorylase inhibitor (5-chloro-6-[1-(2-iminopyrrolidinyl)methyl]uracil hydrochloride, TPI)[18] were generous gifts from Industrial Research Limited (Lower Hutt, New Zealand). Methyl 4,6-*O*-benzylidene-β-D-glucopyranoside (HDH Pharma, San Diego, CA), tetrabutylammonium bisulfate (Fluka), and 2-deoxyribose (dRib, Acros) were purchased commercially. Ultima Gold scintillation fluid (Perkin-Elmer) was used for all scintillation counting. Acetonitrile, methanol, trifluoroacetic acid, and 14.6 cm glass Pasteur pipettes for charcoal columns were purchased from Fisher. Ribonucleotide-triphosphate reductase was a generous gift from Gary Gerfen (Albert Einstein College of Medicine).[19,20] Ribokinase,[21] phospho-D-ribosyl-1-pyrophosphate synthase,[21] and adenine phosphoribosyltransferase[22] were prepared as described previously. All other reagents and synthetic enzymes were from Sigma-Aldrich.

Preparation of hTP. The synthetic gene encoding hTP was purchased in an expression vector from DNA 2.0. The hTP gene was subcloned into the pTWIN1 intein expression vector (New England Biolabs), resulting in a construct with an N-terminal chitin binding domain[23] fused to a mini-intein derived from the *Synechocystis sp* DnaB intein[24] followed by the hTP gene. As per the vector protocol, hTP was subcloned in such a way as to leave no vector derived amino acids after intein cleavage during the enzyme purification. The hTP construct was overexpressed in the K BR2566 (T7 express) cell strain of *Escherichia coli* (New England Biolabs). A typical expression is described as follows: Cells were grown in 1 L baffled flasks containing LB broth and 100 μg/mL carbenicillin at 37 °C to an OD_{600} of 0.7 with shaking. After sufficient cell density was reached, cells were placed at 4 °C for 30 min, augmented with 1 mM IPTG, and shaken at 16 °C and 150 rpm for 24 h. Cells were harvested by centrifugation and frozen in liquid nitrogen. A typical expression resulted in approximately 3 g of cells per 1 L of culture. Cells were thawed and resuspended in chilled buffer containing 100 mM HEPES pH 8.5, 1 mM EDTA, and Roche Mini-Complete, EDTA-free protease inhibitor cocktail (1 pill/10 mL buffer) at a ratio of 1 g of cells/4 mL of lysis buffer. During the entire purification, the enzyme preparation was maintained at 4 °C. Cells were lysed with 3 passes through a French press. The sample was clarified by centrifugation and loaded onto 20 mL of chitin affinity resin (New England Biolabs) in a 3 cm diameter column pre-equilibrated with loading buffer containing 20 mM HEPES pH 8.5, 500 mM NaCl, and 1 mM EDTA at a flow rate of 2 mL/min. The column was washed with 15 column volumes of loading buffer at a rate of 4−6 mL/min. After washing, the column was equilibrated with 10 column volumes of cleavage buffer containing 20 mM sodium phosphate pH 6.5, 500 mM NaCl, and 1 mM EDTA at a flow rate of 6 mL/min. After equilibration, the pH of the eluent was found to be 6.5. The column was incubated in the cold room overnight, and the cleaved hTP was eluted at a rate of 2 mL/min. The enzyme was detected by SDS-PAGE and was electrophoretically homogeneous. The enzyme was concentrated by ultrafiltration to ~20 mg/mL as determined by the calculated molar extinction coefficient of 23,490 M^{-1} cm^{-1} at 280 nm. The concentrated enzyme was dialyzed against 20 mM potassium phosphate buffer at pH 7, aliquoted, and frozen in glass vials with liquid-nitrogen-cooled isopentane. A typical expression yielded 5 mg of hTP/L of culture with a specific activity of 10 U/mg at 22 °C for the phosphorolysis of dT as measured by the Cary 300 spectrophotometric assay (see below).

Because stock enzyme is stored in phosphate to increase stability, a routine dialysis method was developed. Before use in any experiment, stock enzyme was thawed on ice, inserted into a 0.5 mL dialysis cassette, and dialyzed against argon-saturated 20 mM HEPES pH 7.4 buffer at 4 °C with 7 × 300 mL exchanges over 20 h. A constant stream of argon was bubbled through the buffer during dialysis.

Nucleotide and Nucleoside HPLC. A three-step preparative method was developed to purify all radiolabeled nucleosides and nucleotides using a Waters 600C HPLC outfitted with a model 486 UV detector. Samples were monitored at 260 nm and run at a flow rate of 1 mL/min. The first step was also used as an analytical method for quantification of nucleoside related products.

In the first step, reaction products were separated on a 4.6 mm × 250 mm Waters YMC ODS-A analytical C_{18} reversed phase column (5 μm particle size) using a gradient of solvent A (100 mM potassium phosphate buffer pH 6.0 and 6 mM tetrabutylammonium bisulfate) and solvent B (100 mM potassium phosphate buffer pH 6.0 and 6 mM tetrabutylammonium bisulfate in 30% acetonitrile). Separation proceeded with the following elution program: isocratic 100% A for 5 min, ramp to 30:70 A/B over 25 min, isocratic 30:70 A/B for 10 min. Samples were collected and evaporated to a small volume for reinjection.

In the second step, reaction products were separated on a 4.6 mm × 250 mm Waters Delta Pak analytical C_{18} reversed phase column (15 μm particle size) using a gradient of solvent A (water) and solvent B (50% methanol). Separation used the elution program

(16) Guthrie, R. D.; Jencks, W. P. *Acc. Chem. Res.* **1989**, *22*, 343–349.
(17) Birck, M. R.; Schramm, V. L. *J. Am. Chem. Soc.* **2004**, *126*, 2447–2453.
(18) Matsushita, S.; Nitanda, T.; Furukawa, T.; Sumizawa, T.; Tani, A.; Nishimoto, K.; Akiba, S.; Miyadera, K.; Fukushima, M.; Yamada, Y.; Yoshida, H.; Kanzaki, T.; Akiyama, S. *Cancer Res.* **1999**, *59*, 1911–1916.
(19) Blakley, R. L. *Methods Enzymol.* **1978**, *51*, 246–259.
(20) Booker, S.; Stubbe, J. *Proc. Natl. Acad. Sci. U.S.A.* **1993**, *90*, 8352–8356.
(21) Merkler, D. J.; Kline, P. C.; Weiss, P.; Schramm, V. L. *Biochemistry* **1993**, *32*, 12993–13001.
(22) Shi, W.; Tanaka, K. S.; Crother, T. R.; Taylor, M. W.; Almo, S. C.; Schramm, V. L. *Biochemistry* **2001**, *40*, 10800–10809.
(23) Chong, S.; Mersha, F. B.; Comb, D. G.; Scott, M. E.; Landry, D.; Vence, L. M.; Perler, F. B.; Benner, J.; Kucera, R. B.; Hirvonen, C. A.; Pelletier, J. J.; Paulus, H.; Xu, M. Q. *Gene* **1997**, *192*, 271–281.
(24) Wu, H.; Xu, M. Q.; Liu, X. Q. *Biochim. Biophys. Acta* **1998**, *1387*, 422–432.

Table 1. Radiolabeled Starting Material Used To Synthesize Isotopically Enriched Thymidines and Reporter Labels

radiolabeled thymidine	starting material	reporter label
[1′-^{14}C]dT	[1-^{14}C]ribose	[4′-^{3}H]dT, [5′-^{3}H]dT[a]
[1-^{15}N, 5′-^{14}C]dT	[6-^{14}C]glucose[b]	[4′-^{3}H]dT, [5′-^{3}H]dT[a]
[1′-^{3}H]dT	[1-^{3}H]ribose	[5′-^{14}C]dT
[2′*R*-^{3}H]dT	[2*R*-^{3}H]-2-deoxyribose	[5′-^{14}C]dT
[2′*S*-^{3}H]dT	[2*S*-^{3}H]-2-deoxyribose	[5′-^{14}C]dT
[4′-^{3}H]dT	[5-^{3}H]glucose	[5′-^{14}C]dT
[5′-^{3}H]dT	[6-^{3}H]glucose	[5′-^{14}C]dT
[5′-^{14}C]dT	commercially available	n.a.[c]

[a] Both radiolabeled thymidines were used as reporter labels in independent experiments. [b] 1-^{15}N labeled thymine was also used in the synthesis. [c] The KIE of [5′-^{14}C]dT is assumed to be unity (see text).

detailed above. Samples were collected and evaporated to a small volume for reinjection.

In the third step, reaction products were separated on the Waters Delta Pak column (see above) using a gradient of solvent A (50 mM ammonium formate pH 4.1) and solvent B (50 mM ammonium formate pH 4.1 in 50% methanol). Separation used the following elution program: isocratic 100% A for 5 min, ramp to 95:5 A/B over 5 min, ramp to 25:75 A/B over 20 min, ramp to 100% B over 5 min. Samples were evaporated to dryness and resuspended in H_2O repeatedly to remove ammonium formate buffer.

Synthesis of Radiolabeled dT. Except for the 5′-^{3}H and 2′-^{3}H labels, dTs were synthesized in three steps via ATP and dATP. ATPs were synthesized from ^{3}H and ^{14}C labeled glucose or ribose based on an enzymatic synthesis described previously.[17,25] Labels and their starting material can be found in Table 1. [2′*R*-^{3}H]- and [2′*S*-^{3}H]dRib were synthesized chemically in three steps (involving radioincorperation through lithium aluminum tritide reduction) starting from methyl 4,6-*O*-benzylidene-α-D-glucopyranoside and methyl 4,6-*O*-benzylidene-*β*-D-glucopyranoside, respectively. Labeled 2-deoxyribose was converted to dT enzymatically. Details of all procedures can be found in the Supporting Information. [5′-^{3}H]dT was commercially available. All radiolabeled dTs were purified by the preparative HPLC method.

Kinetics of Hydrolysis. The hydrolytic activity of hTP was monitored in a discontinuous assay by following thymine production using the analytical HPLC method. Nucleoside product concentrations were determined by integration of total peak area using the Waters Empower 2 software (version 2154) from the absorbance output measured at 260 nm and compared to a standard curve created with authentic material.

The steady state kinetic parameters for the hydrolysis of dT by hTP at 22 and 37 °C were characterized using the discontinuous assay. A 50 μL reaction mixture with 20 mM HEPES buffer pH 7.4, varying [dT], and 9 μM (22 °C) or 15 μM (37 °C) hTP was incubated at the appropriate temperature, and at periodic intervals 15 μL aliquots were quenched in 2 μL of trifluoroacetic acid. Samples were loaded onto a Waters 717plus autosampler, and 10 μL injections were made. Apparent K_M and k_{cat} were determined using the Michaelis−Menten equation.

Kinetics of hTP Phosphorolysis. A 1 mL solution of 20 mM HEPES, 50 mM potassium phosphate, and 1 mM dT at pH 7.4 was placed in a 1 cm^{-1} path length quartz cuvette, combined with ~50 nM hTP, and then placed in a Cary 300 spectrophotometer. The reaction progress was monitored by the decrease in absorbance of dT upon depyrimidination at 290 nm using an extinction coefficient of $\Delta\varepsilon_{290} = 1000$ M^{-1} cm^{-1}.

A model SX-20 stopped-flow spectrometer (Applied Photophysics) outfitted with a mercury−xenon lamp was used to follow the phosphorolytic depyrimidination of dT by hTP in order to capture the initial velocity period of the steady state at low substrate concentrations, while still maintaining enough hTP to accurately measure the rate. In the reaction chamber, 20 mM HEPES pH 7.4, 1 mM DTT, and varying concentrations of dT or potassium phosphate under saturating concentrations of the second substrate (2.5 mM potassium phosphate or 0.5 mM dT, respectively) were monitored for hTP-catalyzed phosphorolysis using the parameters described above. hTP concentration was maintained at 175 nM (22 °C) or 90 nM (37 °C) in the assay. Apparent K_M and k_{cat} values were determined using the Michaelis−Menten equation.

Characterization of hTP Hydrolysis Products. A hydrolysis reaction was performed with 1 mL of argon-purged 2 mM HEPES buffer pH 7.4, 4 mM dT, and 15 μM hTP in a gastight cuvette at 22 °C overnight. Products were separated using the analytical HPLC method. dRib, which eluted with the solvent front, was characterized with ^{1}H NMR in D_2O by comparing its spectrum to that of authentic material. Thymine was also characterized by ^{1}H NMR in a similar fashion as well as by HPLC coinjection with authentic material.

Determination of KIEs by Scintillation Counting. Competitive KIEs for substrate isotopically enriched with either ^{3}H or ^{14}C at various positions were measured for the hydrolytic reaction catalyzed by hTP. The isotopic label of interest was mixed with the reporter label listed in Table 1 at a CPM ratio of 2:1 ^{3}H/^{14}C. KIEs were determined by measuring the difference in the ^{3}H/^{14}C ratio of products from a partially reacted sample and a reaction taken to completion.[25] In a typical experiment, a 500 μL reaction contained 20 mM HEPES pH 7.4, 3 mM cold carrier dT, and the appropriate pair of radiolabels (using 5×10^5 cpm of ^{14}C). The reaction was initiated with the addition of approximately 10 μM hTP. The reaction was split by removing a 250 μL aliquot and augmenting it with 45 mM AsO_4. hTP performs the irreversible arsenolytic depyrimidination of dT and was used to drive the reaction to completion. After incubation for 1 h at 22 °C, 40 μL samples (6 from each reaction mixture) were loaded onto activated charcoal columns poured in 14.6 cm glass Pasteur pipettes plugged with glass wool. Charcoal columns contained ~1.3 mL of a 4:1 cellulose/charcoal resin poured from a slurry in 10 mM dRib wash buffer. After the sample entered the charcoal bed, the wall of the pipet was rinsed with 3 × 40 μL of wash buffer. Next, 1 mL of wash buffer was added to the column and eluted. The wash step was followed by 3 × 1 mL elution steps using wash buffer augmented with 10% ethanol. All elution steps from one column were collected directly into one scintillation vial. Samples were dried on a centrifugal evaporator, resuspended in 200 μL of H_2O, mixed with 10 mL of scintillation fluid, and measured by scintillation counting.

^{3}H/^{14}C ratios were determined by counting samples for 10 × 5 min in a dual channel scintillation detector (Wallac Winspectral model 1414) and using an appropriate ^{14}C standard to relate channel cpm to total cpm from either radiolabel. The fractional extent of the reaction was determined radiometrically by comparing the reporter label in the partially and totally reacted samples. Fractional and partially reacted samples were verified by the analytical HPLC method on 15 μL aliquots quenched in 2 μL of trifluoroacetic acid. Observed KIEs were calculated according to eq 1.

$$\mathrm{KIE} = \frac{\log(1 - f)}{\log(1 - fR_p/R_0)} \quad (1)$$

where f is the fractional extent of the reaction and R_p and R_0 are the isotope ratios in the product at fractional and total reaction, respectively.

Computational Methods. The hydrolytic reaction of thymidine catalyzed by hTP was studied using the B3LYP method with a 6-31G* basis set.[26] Starting reactants, intermediate, and product geometries were located as global minima, and frequency calculations performed on these optimized geometries had no imaginary frequencies. All transition structures located, with and without geometric constraints, were found to have only one imaginary

(25) Parkin, D. W.; Leung, H. B.; Schramm, V. L. *J. Biol. Chem.* **1984**, *259*, 9411–9417.

(26) Becke, A. D. *J. Chem. Phys.* **1993**, *98*, 5648–5652.

Table 2. Steady State Kinetic Parameters for the Hydrolytic and Phosphorolytic Depyrimidination of dT by hTP

condition[a]	k_{cat} (s^{-1})	K_{dT}[b] (μM)	K_{PO_4}[b] (μM)	k_{cat}/K_{dT} (M^{-1} s^{-1})
Phosphorolysis, 22 °C	2 ± 0.1	31 ± 6	5 ± 0.6	$(6.7 \pm 1.3) \times 10^4$
Hydrolysis, 22 °C	0.04 ± 0.003	820 ± 140	n. a.[c]	50 ± 9
Phosphorolysis, 37 °C	7 ± 0.2	30 ± 4	11 ± 2	$(2.3 \pm 0.3) \times 10^5$
Hydrolysis, 37 °C	0.17 ± 0.02	$(3.7 \pm 0.7) \times 10^4$	n. a.[c]	5 ± 1

[a] hTP assays were at 22 or 37 °C, and steady state kinetic parameters determined as described. [b] In phosphorolysis, the apparent K_M was determined for varying concentrations of substrate at a saturating concentration of the other substrate. [c] Phosphate is not involved in the hydrolytic reaction (see text).

frequency, characteristic of true potential energy saddle points. In order to accurately predict the experimental KIEs, a series of fixed distance optimizations were performed resulting in a grid of possible transition structures for each of the models explored. Geometric constraints were placed only along the reaction coordinate (the forming C−O bond and the breaking C−N bond), and each computed structure was completely relaxed in all other dimensions. Isotope effects were calculated for each of these transition structures using QUIVER,[27−29] and a one-dimensional infinite parabola correction was applied to account for tunneling contributions.[30] For the majority of models explored, a truncated active site histidine mimic (imidazole) representing His116 was also included in addition to thymidine and the water nucleophile (see below). The best-fit model was recalculated using the B3LYP/6-31+G** method; the final model and predicted KIEs are based on this level of calculation.

Results and Discussion

Steady State Characterization of dT Catalysis. hTP catalyzes the hydrolytic depyrimidination of dT to dRib and thymine (Figure 1). Initial rates for the reaction were collected at varying concentrations of dT at pH 7.4 and 22 °C (KIE experimental condition) and 37 °C (Supporting Information). Michaelis−Menten kinetics were observed, and values for apparent K_{dT}, k_{cat}, and catalytic efficiency (k_{cat}/K_{dT}) were decreased by 2 to 4 orders of magnitude with respect to phosphorolysis (Table 2). Hydrolytic turnover by hTP was 2 orders of magnitude more rapid than that reported for bovine and human purine nucleoside phosphorylases,[31,32] consistent with the relative chemical stability of ribonucleosides and deoxyribonucleosides.

The kinetic values for hTP were obtained in continuous assays (Supporting Information) and differ from the wide range of values reported previously.[33] While k_{cat} for the hydrolytic reaction is 40 times lower than that of the phosphorolytic reaction, the k_{cat}/K_{dT} for the hydrolytic reaction is 4.6×10^4 less than that for the phosphorolytic reaction at 37 °C. At 37 °C, the K_{dT} is 1200-fold more favorable in the presence of phosphate (Table 2).

The slow turnover for hydrolysis results from a slow chemical step following weak binding of dT. When substrate binding and release are rapid relative to catalysis, the Michaelis constant approximates the dissociation constant (K_d) for dT. The weak affinity of hTP for dT in the hydrolytic reaction is consistent with the report of a partially open active site in the absence of phosphate; the binding of phosphate triggers partial domain closure and accounts for the large change in K_{dT} for the hydrolysis reaction.[34] These features of the reaction are consistent with a random sequential mechanism with initial binding of phosphate as the preferred pathway.

The possibility that hydrolytic activity was due to a contaminating hydrolase was investigated. In the presence of TPI, a specific nM inhibitor for hTP,[18] no hydrolytic activity was observed (Supporting Information). When hydrolysis was assayed under saturating phosphate conditions (10 mM), the reaction rapidly achieved equilibrium with no further production of thymine under extended incubation (Supporting Information). Therefore, the hydrolytic reaction is catalyzed by hTP.

Corrections to Observed KIEs. Experimental determination of competitive KIEs give apparent isotope effects on k_{cat}/K_M and reflect all steps up to and including the first irreversible step.[35,36] The rate of hTP hydrolysis is dominated by a slow, irreversible chemical step, the enzyme exhibits weak binding of substrate, and at least one of the KIEs is near the theoretical limit. These factors simplify the interpretation of intrinsic KIEs, as bond breaking dominates the apparent KIEs.

The observed KIEs for positions of interest were corrected for the KIE on the reporter label. The apparent KIE for 5′-^{14}C is assumed to be unity as it is three bonds removed from the reaction center and ^{14}C does not manifest significant isotope effects for geometric changes or binding (in contrast to reporter ^{3}H labels).[37,38] Nucleosidases are known to exhibit isotope effects for remote ^{3}H atoms,[14] and corrections to the observed KIEs were required (Tables 1, 3).

KIEs for dT Hydrolysis. Intrinsic KIEs reflect the nature of the transition state at the kinetically significant (rate-determining) chemical step.[35,36] Experimental KIEs for the hTP-catalyzed hydrolysis of dT are listed in Table 3.

1-^{15}N KIE. The near-unity 1-^{15}N KIE reports on the rehybridization of the N1 position of thymidine as a result of the altered C1′-N1 bond order. A small nitrogen KIE can be explained by preservation of the bond order or by no participation of the leaving group. This phenomenon can arise with (1) an early concerted bimolecular A_ND_N mechanism with minimal bond breakage to the leaving group nitrogen, (2) an early

(27) Saunders, M.; Laidig, K. E.; Wolfsberg, M. *J. Am. Chem. Soc.* **1989**, *111*, 8989–8994.
(28) All frequencies were scaled by 0.9614.
(29) Scott, A. P.; Radom, L. *J. Phys. Chem.* **1996**, *100*, 16502–16513.
(30) Bell, R. P. *The Tunnel Effect in Chemistry*; Chapman & Hall: London, 1980; pp 6063.
(31) Kline, P. C.; Schramm, V. L. *Biochemistry* **1992**, *31*, 5964–5973.
(32) Ghanem, M.; Murkin, A. S.; Schramm, V. L. *Chem. Biol.* **2009**, *16*, 971–979.
(33) Desgranges, C.; Razaka, G.; Rabaud, M.; Bricaud, H. *Biochim. Biophys. Acta* **1981**, *654*, 211–218. Sugata, S.; Kono, A.; Hara, Y.; Karube, Y.; Matsushima, Y. *Chem. Pharm. Bull. (Tokyo)* **1986**, *34*, 1219–1222. Finnis, C.; Dodsworth, N.; Pollitt, C. E.; Carr, G.; Sleep, D. *Eur. J. Biochem.* **1993**, *212*, 201–210. Kouni, M. H.; Kouni, M. M.; Naguib, F. N. *Cancer Res.* **1993**, *53*, 3687–3693. Miszczak-Zaborska, E.; Wozniak, K. *Z. Naturforsch. C* **1997**, *52*, 670–675. van Kuilenburg, A. B.; Zoetekouw, L. *J. Chromatogr. B* **2005**, *820*, 271–275.
(34) Pugmire, M. J.; Cook, W. J.; Jasanoff, A.; Walter, M. R.; Ealick, S. E. *J. Mol. Biol.* **1998**, *281*, 285–299.
(35) Cook, P. F.; Cleland, W. W. *Enzyme Kinetics and Mechanism*; Garland Science: New York, 2007; pp 253−323.
(36) Northrop, D. B. *Annu. Rev. Biochem.* **1981**, *50*, 103–131.
(37) Lewis, B. E.; Schramm, V. L. *J. Am. Chem. Soc.* **2001**, *123*, 1327–1336.
(38) Lewis, B. E.; Schramm, V. L. *J. Am. Chem. Soc.* **2003**, *125*, 4785–4798.

Table 3. Experimental Competitive KIEs for the Hydrolytic Depyrimidination of dT by hTP

labeled dT	type of KIE	apparent KIE[a,b]
[1′-^{14}C]dT	primary ^{14}C	1.033 ± 0.002 (4)[c]
[1-^{15}N, 5′-^{14}C]dT	primary ^{15}N	1.004 ± 0.002 (4)[c]
[1′-^{3}H]dT	α-secondary ^{3}H	1.325 ± 0.003 (4)
[2′*R*-^{3}H]dT	β-(*R*)-secondary ^{3}H	1.101 ± 0.004 (3)
[2′*S*-^{3}H]dT	β-(*S*)-secondary ^{3}H	1.087 ± 0.005 (3)
[4′-^{3}H]dT	γ-secondary ^{3}H	1.040 ± 0.003 (2)
[5′-^{3}H]dT	δ-secondary ^{3}H	1.033 ± 0.003 (2)

[a] The number in parentheses is the number of independent KIE experiments. [b] The experimentally measured KIE for the position of interest (corrected for reporter label where noted) is equal to the apparent KIE (see text). [c] KIEs were corrected for the reporter ^{3}H label according to the expression: $KIE_{app} = KIE_{obs} \times KIE_{report}$, where KIE_{app} is the apparent KIE for the position of interest, KIE_{obs} is the experimentally measured KIE, and KIE_{report} is the observed KIE for the reporter label.

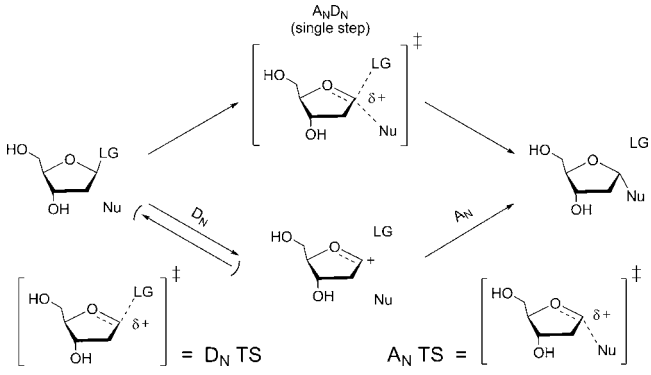

Figure 2. Generic mechanism for glycosidic bond cleavage of ribofuranosides. In the upper pathway, attack from the nucleophile (Nu) displaces the leaving group (LG) in a concerted bimolecular process (A_ND_N). In the lower pathway, departure of LG occurs in an independent step (D_N) from attack of the 2-deoxyribocation by Nu (A_N). D_N TS is the transition state for the D_N step, and A_N TS is the transition state for the A_N step. In a $DN^*A_N^{\ddagger}$ mechanism, the A_N step is rate-limiting, and the glycosidic bond cleaves and reforms many times before nucleophilic capture.

stepwise $D_N^{\ddagger}{*}A_N$ mechanism with substantial bond order to the leaving group nitrogen in the kinetically significant step, or (3) a stepwise $D_N{*}A_N^{\ddagger}$ mechanism where the intermediate is in equilibrium with reactants and there is no participation of the leaving group at the rate-determining step. The dissociative A_ND_N and stepwise $D_N{*}A_N$ mechanisms known for *N*-glycoside hydrolysis and transfer reactions of 2′-deoxynucleosides are shown in Figure 2. In stepwise reactions involving thymidine, a 2-deoxyribocation intermediate is formed. The high energy nature of the oxocarbenium ion makes an early $D_N^{\ddagger}{*}A_N$ mechanism unlikely and implies no participation of thymine at the TS.

1′-^{3}H KIE. The α-secondary 1′-^{3}H KIE of 1.325 is indicative of a ribocation-*like* transition state. Rehybridization at the anomeric carbon to sp^2 results from either stepwise or dissociative bimolecular mechanisms. The α-secondary KIE argues against early A_ND_N or early $D_N^{\ddagger}{*}A_N$ mechanisms, as these would exhibit smaller 1′-^{3}H KIE values. Rehybridization of C1′ from sp^3 to sp^2 and loss of steric hindrance from an absent leaving group give increased freedom to the out-of-plane bending mode of H1′ resulting in a large normal KIE.[39,40] Considered with the 1-^{15}N KIE, the transition state appears to include full loss of thymine and near-full ribocation character.

2′-^{3}H KIEs. The magnitudes of the β-secondary KIEs reflect the geometry of the ribose ring. The π-bonding character in the O4′−C1′ bond of the 2-deoxyribocation favors coplanarity of the C4′−O4′−C1′−C2′ atoms and consequently a 3′-*endo* or 3′-*exo* ring conformation. Transition states involving highly developed ribocations in the 3′-*exo* conformation give rise to tritium KIEs equal to or greater than 1.1 at the 2′*S* position from significant hyperconjugation between the C2′−H2′ σ-bond and the vacant p-orbital of C1′. This increases the π-bond character in the C1′−C2′ bond and weakens the C2′−H2′ σ-bond, where the magnitude of the KIE observed increases with optimization of orbital alignment[41,42] (e.g., see Berti and McCann[14]). A similar trend is observed for tritium KIEs at the 2′*R* position when the ribocation is in the 3′-*endo* conformation.[43−45] The β-(*R*)-secondary (1.101) and β-(*S*)-secondary (1.087) ^{3}H KIEs indicate significant ribocation character. The similar and large stereospecific β-secondary KIEs indicate strong hyperconjugation from both C2′−H2′ bonds, while the absolute values favor a mild 3′-*endo* sugar pucker. An alternative explanation is a broad saddle point for this reaction, where barrier crossing with both 3′-endo and 3′-exo geometry is permitted.

1′-^{14}C KIE. Primary ^{14}C KIEs for *N*-glycoside hydrolysis and transfer reactions range from 1.0 to 1.03 for reactions involving ribocation transition states and from 1.08 to 1.13 for associative neutral transition states.[11] The apparent KIE of 1.033 supports ribocation character at the TS.

Steps Contributing to Apparent KIEs. The $D_N{*}A_N^{\ddagger}$ mechanism involves departure of the leaving group followed by slower attack of the nucleophile occurring in a separate step. In this mechanism the reaction proceeds through a fully formed, discrete intermediate in equilibrium with reactants. The kinetic mechanism for the hydrolytic process (shown through the release of the first product) is described by eq 2.

$$E + A \underset{k_2}{\overset{k_1}{\rightleftharpoons}} E \cdot A \underset{k_4}{\overset{k_3}{\rightleftharpoons}} [E \cdot O] \xrightarrow{k_5} E \cdot P \cdot Q \xrightarrow{k_7} E \cdot Q + P \tag{2}$$

O is the oxocarbenium ion intermediate. In hydrolysis, it is not known which is the first product to release; therefore P and Q are left unassigned. The equation for competitive KIEs expressed in eq 2 has been derived from the equation describing k_{cat}/K_M (eq 3).[11,44] The apparent KIEs are a function of partitioning of the ribocation into reactant (k_4) and product (k_5).

$$KIE = \frac{\frac{\alpha_1\alpha_3}{\alpha_2}\left(\frac{\alpha_5}{\alpha_4} + \frac{k_5}{k_4}\right)}{1 + \frac{k_5}{k_4}} \tag{3}$$

where α_n is the intrinsic KIE for step *n*. For the $D_N{*}A_N^{\ddagger}$ mechanism described here, the intermediate is in equilibrium

(39) Glad, S. S.; Jensen, F. *J. Am. Chem. Soc.* **1997**, *119*, 227–232.
(40) Matsson, O.; Westaway, K. C. In *Advances in Physical Organic Chemistry*; Bethell, D., Ed.; Academic Press: San Diego, 1998; Vol. 31, pp 143−248.
(41) Mentch, F.; Parkin, D. W.; Schramm, V. L. *Biochemistry* **1987**, *26*, 921–930.
(42) Sunko, D. E.; Szele, I.; Hehre, W. J. *J. Am. Chem. Soc.* **1977**, *99*, 5000–5005.
(43) Chen, X.-Y.; Berti, P. J.; Schramm, V. L. *J. Am. Chem. Soc.* **2000**, *122*, 1609–1617.
(44) Chen, X.-Y.; Berti, P. J.; Schramm, V. L. *J. Am. Chem. Soc.* **2000**, *122*, 6527–6534.
(45) Singh, V.; Lee, J. E.; Nunez, S.; Howell, P. L.; Schramm, V. L. *Biochemistry* **2005**, *44*, 11647–11659.

Scheme 1. Models (A−D) To Explore a Reversible First Step with Equilibrium Formation of a Thymine-Related Intermediate

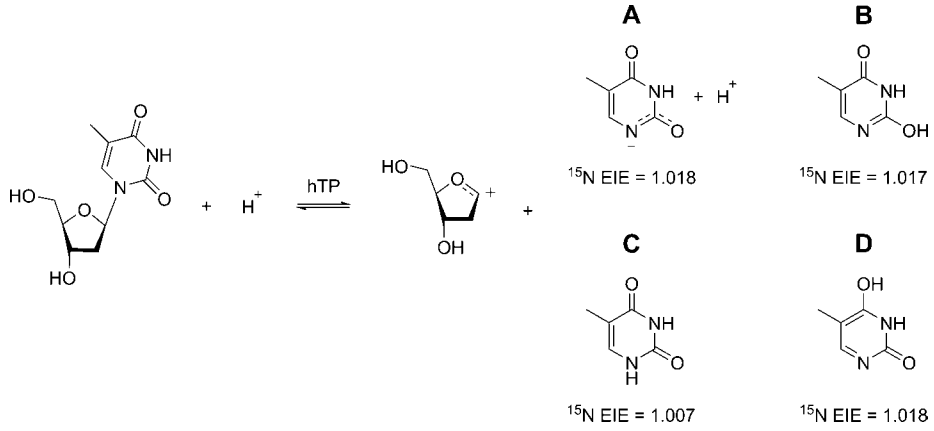

with the reactant, k_5 is the first irreversible step, and $k_4 \gg k_5$. Under these conditions eq 3 simplifies to eq 4.

$$\mathrm{KIE} = \left(\frac{\alpha_1\alpha_3}{\alpha_2\alpha_4}\right)\alpha_5 \tag{4}$$

where the term $(\alpha_1\alpha_3/\alpha_2\alpha_4)$ is the EIE between reactants free in solution and the intermediate and α_5 is the intrinsic KIE on the rate-determining (A_N) step. For hTP, a test of the transition state model is established computationally by comparison of experimental values to theoretical predictions for all reasonable possibilities.

^{15}N Isotope Effect and Mechanistic Models. A most informative KIE measurement for hTP hydrolysis is the near-unity ^{15}N isotope effect (1.004 ± 0.002; Table 3). This value suggests that there is little or no rehybridization of N1 at the rate-determining transition state. However the KIEs at the center directly bonded to N1 (1′-^{14}C, 1.033 ± 0.002; 1′-^{3}H, 1.325 ± 0.003) are suggestive of significant rehybridization at the transition state. The obvious explanation for this conflicting interpretation is that the ^{15}N KIE and the 1′-^{14}C/1′-^{3}H KIEs have their origins in different chemical steps. To confirm this we explored mechanisms where the C−N bond cleavage was part of a single rate-determining step, namely the A_ND_N and $D_N^{\ddagger}{}^*A_N$ mechanisms (see Supporting Information for KIE predictions of these models). In some models, the possibility of interactions with an active site histidine (His116) was also explored by incorporating a histidine mimic (imidazole). The active site histidine is an essential catalytic residue[46] and has been invoked in an earlier theoretical study on the phosphorolytic reaction catalyzed by the structurally related *E. coli* thymidine phosphorylase,[47] where it was proposed to play the dual role of nucleophile activation and leaving group stabilization (at O2) through hydrogen bonding interactions. The predicted ^{15}N KIEs for these models, with and without the histidine mimic, range from 1.020 to 1.035 and are not in agreement with experimental KIEs.

The $D_N{}^*A_N^{\ddagger}$ mechanism invokes reversible formation of an enzyme-bound thymine-related intermediate and the 2-deoxyribocation followed by rate-limiting capture of the ribocation by a water nucleophile. The experimental consequence of this mechanism makes the ^{15}N KIE an EIE for the reversible formation of the thymine-related intermediate from thymidine (see above). The prediction of the ^{15}N EIE under these circumstances is addressed in Scheme 1A−D. The calculated ^{15}N EIE between free dT and (A) thymine with a stabilized anion at N1 is 1.018, (B) for the 1,2-lactim tautomer of thymine it is 1.017, (C) for N1 protonated thymine it is 1.007, and (D) for the tautomer resulting from protonation at O4 it was 1.018. The value of 1.007 (Scheme 1C) agrees best with the observed ^{15}N KIE. The agreement of the observed ^{15}N KIE to that predicted for Scheme 1C, as well as the disagreement with all other models explored, suggests that hTP hydrolysis proceeds through a $D_N{}^*A_N^{\ddagger}$ mechanism.

That hTP facilitates leaving group departure through favorable hydrogen bonding to O2 raises the possibility that it is the 1,2-lactim form of thymine that is eliminated; a related strategy was observed for the N7 protonation of adenine in the deadenylation reaction of DNA catalyzed by MutY.[48] This hydrogen bonding interaction need not formally protonate O2 during turnover and instead may assist the elimination of thymine as the N1 anion by stabilizing the leaving group. A similar mechanism has been proposed for the hydrolysis of uracil from DNA catalyzed by uracil DNA glycosylase (UDG).[49] The observed EIE between free dT and N1 protonated thymine indicates that bound thymine must either be directly protonated at N1 or tautomerize to the lactam form ahead of nucleophilic attack on the oxocarbenium ion (Figure 3).

Nature of the Nucleophile. Transition state structures for the acid-catalyzed hydrolysis of deoxyadenosine monophosphate (dAMP) and the MutY-catalyzed hydrolysis of DNA have been characterized using multiple KIEs.[48,50] As in the hydrolysis reaction catalyzed by hTP, these reactions are also proposed to proceed via $D_N{}^*A_N^{\ddagger}$ mechanisms. In these three reactions, the A_N step is similar and involves capture of the 2-deoxyribosyl oxocarbenium ion by water. A comparison of 1′-^{14}C and 1′-^{3}H intrinsic KIEs for the A_N step (defined as KIE′) of these hydrolysis reactions is shown in Table 4. The 1′-^{14}C KIE′ for acid-catalyzed dAMP hydrolysis and MutY-catalyzed DNA hydrolysis are similar (MutY is slightly later than dAMP) and have been interpreted as resulting from the attack of water in

(46) Mitsiki, E.; Papageorgiou, A. C.; Iyer, S.; Thiyagarajan, N.; Prior, S. H.; Sleep, D.; Finnis, C.; Acharya, K. R. *Biochem. Biophys. Res. Commun.* **2009**, *386*, 666–670.
(47) Mendieta, J.; Martin-Santamaria, S.; Priego, E.-M.; Balzarini, J.; Camarasa, M.-J.; Perez-Perez, M.-J.; Gago, F. *Biochemistry* **2003**, *43*, 405–414.
(48) McCann, J. A. B.; Berti, P. J. *J. Am. Chem. Soc.* **2008**, *130*, 5789–5797.
(49) Werner, R. M.; Stivers, J. T. *Biochemistry* **2000**, *39*, 14054–14064.
(50) McCann, J. A. B.; Berti, P. J. *J. Am. Chem. Soc.* **2007**, *129*, 7055–7064.

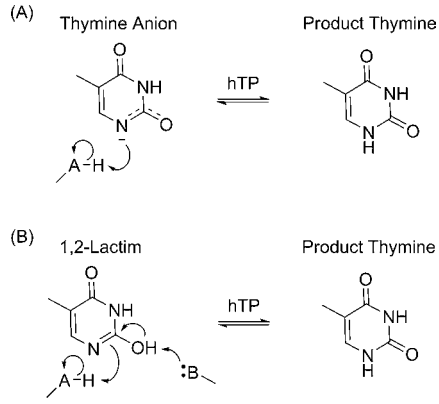

Figure 3. The observed EIE between free dT and N1 protonated thymine (product thymine) indicates that the leaving group undergoes general acid−base chemistry before nucleophilic capture of the oxocarbenium ion intermediate. (A) Direct protonation at N1 if thymine leaves as an anion. (B) Tautomerization of the 1,2-lactim if thymine is formally protonated at O2 as it leaves.

Table 4. Comparison of KIE′[a] for the A_N Step in Acid-Catalyzed dAMP Solvolysis and MutY and hTP Catalyzed Hydrolysis

Position	dAMP[b]	MutY[b]	hTP
1′-^{14}C	1.007	1.012	1.040
1′-^{3}H	0.931	0.855	0.937

[a] The KIE′ was calculated by using the calculated EIE and measured apparent KIE. The apparent KIE = KIE′ * EIE, where KIE′ is the intrinsic KIE on the A_N step and EIE is for the formation of the oxocarbenium ion from the starting material. [b] Data for dAMP[50] and MutY[48] hydrolysis are reproduced from previous reports.

Table 5. Comparison of Calculated KIE′[a] for Second Step Using Three Different Nucleophiles

Position	Water (r_{C-O} = 2.6 Å)	Activated water (r_{C-O} = 2.6 Å)	Hydroxide (r_{C-O} = 2.6 Å)
1′-^{14}C	1.017	1.035	1.044
1′-^{3}H	0.988	0.986	1.023

[a] KIE′ computed using the oxocarbenium ion as the starting material. A 1-D infinite parabola correction was applied to correct for the contribution of tunneling to the predicted KIEs.

an early, rate-limiting transition state.[48,50] The 1′-^{14}C KIE′ for hTP is much larger, supporting a transition state different from dAMP and MutY. This elevated 1′-^{14}C KIE′ might suggest a much later transition state for the attack of water. However, increased nucleophilic participation (later transition state) would cause the 1′-^{3}H KIE′ to become significantly more inverse. This is not observed; the 1′-^{3}H KIE′ for hTP hyrolysis is not sufficiently inverse or significantly different (from dAMP and MutY) to suggest the larger 1′-^{14}C KIE′ is a result of increased nucleophilic participation. An alternate explanation is required to account for the experimental observations.

We hypothesized that the larger 1′-^{14}C KIE′ in the case of the hTP-catalyzed hydrolysis reaction (as compared to the other two reactions) might be due to the increased nucleophilicity of the water nucleophile. We modeled the capture of the 2-deoxyribocation by three different water-related nucleophiles—water, activated water and deprotonated water (hydroxide)—at a fixed carbon−oxygen bond forming distance of 2.6 Å.[51] The KIE′ predictions for these three geometries are shown in Table 5. Changing the nature of the nucleophile had little impact on 1′-^{3}H KIE′. However, the 1′-^{14}C KIE′ doubled in magnitude on going from water to activated water and increased ∼1% on going from activated water to hydroxide.[52] This is because the loss of bond order to the nucleophilic oxygen, on going from water to hydroxide, is compensated by amplified motion along the reaction coordinate. The more general implication of this observation is that, for a given bond order between a nucleophile and an oxocarbenium ion, the magnitude of the primary 1′-^{14}C KIE gives information about not only the extent of bond formation but also the nucleophilicity of the nucleophile at the transition state. This analysis strongly suggests that general base (histidine) activation of water occurs at the rate-determining transition state.

Scheme 2. Model Depicting Capture of the Oxocarbenium Ion by a Water Nucleophile Activated through Hydrogen Bonding Interactions with a General Base (Histidine Mimic) in the Active Site

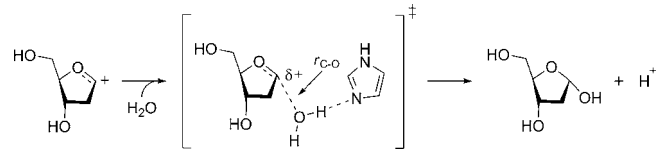

Transition State Model. Within the framework of the D_N*$A_N^{\ddagger}$ mechanism, the KIEs for positions on the 2′-deoxyribose ring are predicted as a combination of the EIEs for the reversible D_N step and the intrinsic KIEs for the A_N step. We modeled capture of the 2-deoxyribocation by a water nucleophile with concomitant activation of the water through hydrogen bonding interactions with a histidine mimic in the active site (Scheme 2); a series of optimized geometries at fixed distances of the forming carbon−oxygen bond were generated (r_{C-O} = 2.0−2.5). Table 6 shows the predicted KIEs for the mechanism along with the respective EIE and KIE′ values. Figure 4 shows the transition structure from which these predictions were made.

Table 6. Predicted Ring KIEs for a D_N*$A_N^{\ddagger}$ Mechanism and Comparison with Experimental KIEs

Position	EIE[a] (D_N)	KIE′[b] (A_N)	calculated KIE[c]	Experimental
1′-^{14}C	0.993	1.039	1.032	1.033 ± 0.002
1-^{15}N	1.007	−	1.007	1.004 ± 0.002
1′-^{3}H	1.413	0.923	1.303	1.325 ± 0.003
2′-^{3}H (*R*)	1.117	0.987	1.102	1.101 ± 0.004
2′-^{3}H (*S*)	1.320	0.863	1.138	1.087 ± 0.005

[a] EIE is calculated for the formation of the oxocarbenium ion and thymine from the starting material. [b] KIE′ is the KIE calculated for the A_N step starting from the intermediate. [c] Calculated KIE = EIE * KIE′

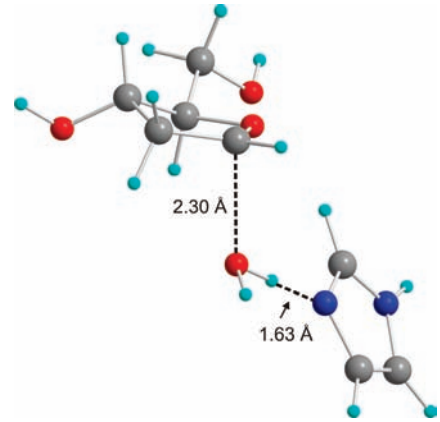

Figure 4. Transition state structure determined for the $A_N^{\ddagger}$ step in the hTP-catalyzed hydrolytic depyrimidination of dT.

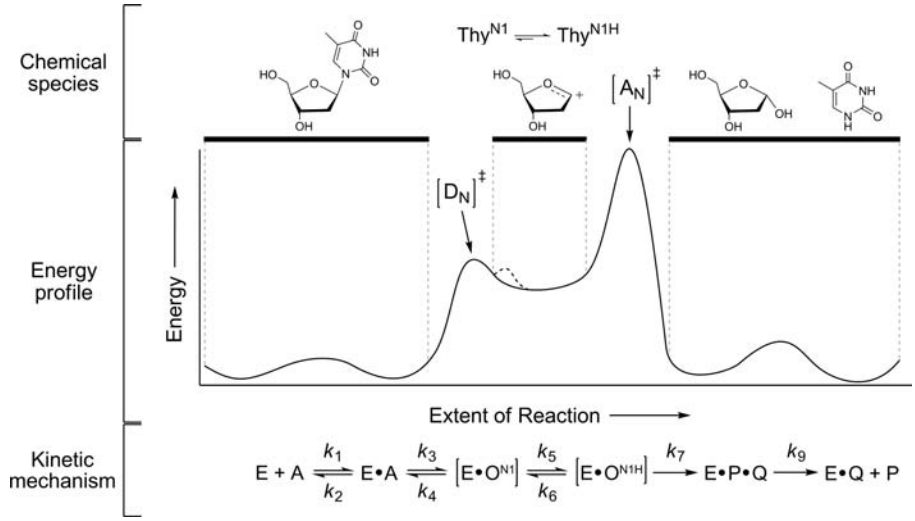

Figure 5. Chemical and kinetic mechanism of the hTP-catalyzed depyrimidination of dT. In the proposed mechanism, departure of the thymine leaving group forms a discrete ribocation intermediate. Thymine likely leaves deprotonated at N1 (Thy^{N1}). The current results suggest that thymine undergoes enzyme-catalyzed protonation at N1 before the next step (Thy^{N1H}). In the following step, the intermediate undergoes nucleophilic attack from an activated water molecule to form products. (Upper panel) The chemical species present at each stage of catalysis. (Middle panel) Free energy profile for the minimally required changes that occur during catalysis represented qualitatively. $[D_N]^‡$ is the transition state for the dissociation of the leaving group, D_N, and $[A_N]^‡$ is the transition state for the rate limiting association of the nucleophile, A_N. The proposed protonation step is represented by the dashed line (- - -). (Lower panel) The minimal kinetic mechanism through release of the first product: E, enzyme free in solution; A, substrate free in solution; E•A, Michaelis complex; $E•O^{N1}$, enzyme• (oxocarbenium ion + eliminated form of thymine in D_N step) intermediate complex; $E•O^{N1H}$, enzyme• (oxocarbenium ion + thymine) intermediate complex; E•P•Q, ternary product complex; E•Q, binary product complex; P, product free in solution; k_n, rate constant on step *n*.

Except for the 2′-^{3}H(*S*) KIE, the quantitative agreement of experimental and theoretical KIEs in Table 6 is remarkable and further supports the mechanistic conclusion. The prediction of a mild 3′-*endo* ring pucker (see KIEs for dT Hydrolysis) is consistent with the transition state geometry (Figure 4). Overprediction of the 2′-^{3}H(*S*) KIE likely results from a limitation in the calculation to account for active site interactions that damp the vibrational modes giving rise to this KIE or from a broad saddle point with respect to 2-deoxyribocation pucker.

Transition States of *N*-Glycosylase Reactions. *N*-Glycoside cleavage of ribofuranosides largely proceed by dissociative A_ND_N mechanisms with a single transition state. Notable exceptions occur. Human and *P. falciparum* purine nucleoside phosphorylase both catalyze stepwise D_N*A_N mechanisms,[53] as does 5′-methylthioadenosine nucleosidase from *E. coli*,[45] 5′-methylthioadenosine nucleosidase from humans,[54] and ricin when catalyzing the hydrolytic deadenylation of small stem-loop RNA.[43] Enzymatic catalysis of the analogous reactions for 2′-deoxyribofuranosides is less well-known. Transition state analyses through KIE measurements have shown that the hydrolytic depurination of DNA catalyzed by ricin[44] and MutY[48] proceeds by $D_N^‡$*A_N and D_N*$A_N^‡$ mechanisms, respectively. UDG has also been shown to promote the stepwise hydrolysis of uracil from DNA with rate-limiting leaving group departure.[49,50] The current study shows that the hydrolytic depyrimidination of dT by hTP follows this trend.

Conclusions

The hydrolytic depyrimidination of dT by hTP proceeds through a stepwise D_N*$A_N^‡$ mechanism, with rate-limiting capture of the 2-deoxyribocation intermediate by a water molecule activated through hydrogen bonding to histidine 116 (Figure 5). The highest energetic barrier in the reaction coordinate results from the weak nucleophilic nature of water and/or its improper alignment relative to phosphate in the normal phosphorolytic reaction. Replacement of phosphate by water may alter the previously reported concerted bimolecular mechanism to a stepwise mechanism with a slow nucleophilic attack.[17] A rate-limiting A_N step indicates that leaving group departure can be catalyzed without phosphate participation. However, phosphate is required for favorable thymidine binding, supporting the proposed role of phosphate in organizing the active site.[34] Most of the hTP catalytic power is independent of nucleophile interactions since hydrolytic turnover is only 40 times lower than the case for phosphorolysis.

Leaving group departure for the phosphorolytic reaction is facilitated through hydrogen bonding to thymine O2 by an active site histidine and must be similar for hydrolysis.[47] The thymine species eliminated from dT is not protonated at N1 and is either the 1,2-lactim tautomer of thymine (formal protonation at O2) or a thymine anion deprotonated at N1. An EIE is established between reactants and N1 protonated thymine before the A_N step (Figure 5). Equilibrium between product thymine and either of the possible elimination species would favor N1 protonated thymine,[55] consistent with the KIE values. A rapid tautomerization could be catalyzed through general acid−base chemistry, and direct protonation of a thymine anion could also occur via an active site residue (Figure 3).

Strategies to facilitate *N*-glycosidase catalysis can include activation of the nucleophile and stabilization of the leaving

(51) We chose 2.6 Å since this was the earliest geometry that gave one imaginary frequency along the reaction coordinate for the three nucleophiles considered.
(52) It must be noted here that a 4% change in a ^{3}H KIE has little mechanistic significance while a 1% (or greater) change in a ^{14}C KIE is significant in the interpretation of the mechanism of a reaction (see: *Isotope Effects in Chemistry and Biology*; Kohen, A., Limbach, H.-H., Eds.; Taylor & Francis: Boca Raton, FL, 2006).
(53) Lewandowicz, A.; Schramm, V. L. *Biochemistry* **2004**, *43*, 1458–1468.
(54) Singh, V.; Schramm, V. L. *J. Am. Chem. Soc.* **2006**, *128*, 14691–14696.

group through protonation or hydrogen bonding interactions. Stabilization of the ribocation by active site residues has been exploited to create families of pM to fM inhibitors for several of these enzymes.[56] Continued application of transition state theory to hTP may be useful in terms of drug development.

Acknowledgment. This work was supported by NIH Research Grant GM41916.

Supporting Information Available: Details for the preparation of radiolabeled dTs; ^{1}H NMR spectra for specifically deuterated species in the chemical synthesis of [2′-^{2}H]dRib; hTP kinetic data; complete calculation results. This material is available free of charge via the Internet at http://pubs.acs.org.

JA105041J

(55) Scanlan, M. J.; Hillier, I. H. *J. Am. Chem. Soc.* **1984**, *106*, 3737–3745.
(56) Schramm, V. L. *J. Biol. Chem.* **2007**, *282*, 28297–28300.